Investigation of ocean acoustics using a pseudospectral time domain model

G. R. Elston, J. M. Bell

Dept. of Computing and Electrical Engineering, Heriot-Watt University, Edinburgh, EH14 4AS, UK.
elstongr@cee.hw.ac.uk , jmb@cee.hw.ac.uk

Abstract

The Pseudospectral time domain method provides a flexible and powerful tool for the modelling and analysis of complex ocean acoustics problems, since it inherently treats all aspects of the problem including complex wave effects. This paper will illustrate the scope of such a model, before concentrating on the ability of the model to calculate the scattering of acoustic waves at complex realistic boundaries, including the scattering due to the surface roughness and the penetration of sound into sediments

1. Introduction

Modelling has an important role in the examination and understanding of ocean acoustical problems. A realistic and accurate model can aid in pre-mission planning and can provide a tool for the analysis of results, the extrapolation of data to alternative environments, or the isolation of individual phenomena. The model presented in this paper is intended to simulate any active sonar system - including bistatic, synthetic aperture, sidescan or bathymetric sonars - in an arbitrary underwater environment. This requires the output of the pressure signals from each transducer which can then be beamformed or otherwise processed to produce synthetic sonar signals and hence images. This in turn demands a very general method incorporating coherence, propagation, multiple reflections and scattering from both rough surfaces and volume inhomogeneities.

One method which can fulfil these requirements is the pseudospectral time domain (PSTD) method, which is a direct extension from classical finite difference time domain (FDTD) techniques. It has the advantages of reducing the computational complexity whilst enhancing their accuracy and scope. These methods are already established in the literature outwith the underwater acoustics field and are therefore only outlined here.

The majority of the paper concentrates on the comprehensive nature of the PSTD method and its suitability for a general sonar model by demonstrating its inherent ability to reproduce the features described above. These effects are automatic once the scene and sonar source have been specified by the user. Furthermore, the output from the model is the full evolution of the pressure field in space and time which allows element-level data to be recorded directly. The first set of experiments are qualitative and show the model performing as expected for interfaces between homogeneous sand, water and air. In the second set, volume inhomogeneities are incorporated into the sand and comparisons made between volume-only, surface-roughness-only and combined surface-volume scattering. This bistatic scattering is then quantified and compared to an established theoretical model.

2. Pseudospectral Time Domain Technique

The pseudospectral time-domain technique is simply an enhancement of classical finite-difference time-domain methods which employs the Fourier transform to calculate field derivatives. FDTD methods are based on the discretisation of a wave equation in which the exact differential operators are replaced by local difference approximations over a discrete space-time grid. For a 2nd order discretisation of the basic 2nd order wave equation, this process leads to the recurrence relation:

$$p_{i,j}^{n+1} = r^2\left(p_{i-1,j}^{n} + p_{i+1,j}^{n} + p_{i,j-1}^{n} + p_{i,j+1}^{n}\right) + 2(1-r^2)p_{i,j}^{n} - p_{i,j}^{n-1} \qquad (1)$$

where the mesh ratio $r = c\Delta t / \Delta x$; c is the local sound speed;and $p_{i,j}^{n} = p(i\Delta x, j\Delta y, n\Delta t)$ is the pressure as a function of range ($i\ \Delta x$), depth ($j\ \Delta y$) and time ($n\ \Delta t$) for integers i, j and n. The pressure at a given point in space and time is calculated from the values at local points in the previous two time steps; thus iteration of (1) yields the full spatial and temporal evolution of the acoustic field.

The most significant advantage of this technique is its inherent capability to calculate all aspects of the sonar process, such as propagation; losses; refraction and other wave effects (including diffraction); and reflections at surfaces with appropriate boundary conditions. In addition, realistic source and receiver elements can be

TG Leighton, GJ Heald, HD Griffiths, G Griffiths, (eds.), 'Acoustical Oceanography', Proc. Institute of Acoustics Vol. 23 Part 2, 2001.

positioned anywhere within the scene and the time series obtained across the distributed array. This has previously been illustrated for the 2nd order FDTD scheme (1) in [1].

The main disadvantage of the FD method is the huge computational effort involved in its calculation. Sub-wavelength/period discretisation is necessary (in space/time) in order for the solution to remain stable. Typically a minimum of 10 points per wavelength (PPW) is required for a 2nd order scheme [2], although practically a much higher discretisation is required to minimise the numerical dispersion. The number of PPW can be reduced by deriving a recurrence relation from a higher-order discretisation of the wave equation.

The pseudospectral time domain (PSTD) method is strongly related to FDTD and essentially represents the "infinite-order" limit of FDTD schemes [3]; thus it remains stable and accurate up to the Nyquist limit of 2 PPW. Simulations of larger environments and higher frequencies are therefore possible for the same computational load. The PSTD method also virtually eliminates the numerical dispersion associated with FDTD schemes. Instead of approximating the spatial derivatives by local differences as for FDTD methods, the PSTD technique calculates them exactly using the global Fourier transform (FT):

$$f'(x) = FT^{-1}\left[\iota k FT\left[f(x)\right]\right] \tag{2}$$

where $f(x)$ and $f'(x)$ are the spatial fields and their derivatives; k is the wavenumber; and ι is the imaginary number. In order to prevent the solution from wrapping around the boundaries due to the periodic nature of the FFT, the perfectly matched layer (PML) absorbing boundary condition (ABC) [4] is employed at the exterior boundaries of the numerical domain. This PML ABC also acts to prevent spurious reflections from the exterior edges of the numerical domain.

The PSTD scheme that has been implemented solves the following coupled first-order wave equation (3):

$$\rho\frac{\partial \mathbf{v}(\mathbf{r},t)}{\partial t} = -\nabla p\,, \qquad \frac{\partial p}{\partial t} + \gamma(\mathbf{r})c^2(\mathbf{r})p(\mathbf{r},t) = -\rho(\mathbf{r})c^2(\mathbf{r})\nabla\cdot\mathbf{v}(\mathbf{r},t) + f_s(\mathbf{r},t) \tag{3}$$

where $\mathbf{v}(\mathbf{r},t)$ is the fluid velocity at position $\mathbf{r}$; and the sound speed c, density ρ and absorption coefficient γ define the local material. The two-step recursion relation for solving the wave equation (3), including the PML, is similar in form and function to (1). As it is lengthy and involved it is not repeated here, but it is clearly derived in [4]. Essentially the method works because it is a direct numerical solution of the wave equation, therefore an impedance contrast between materials causes reflection from and transmission through the boundary; it also causes scattering if this boundary is rough.

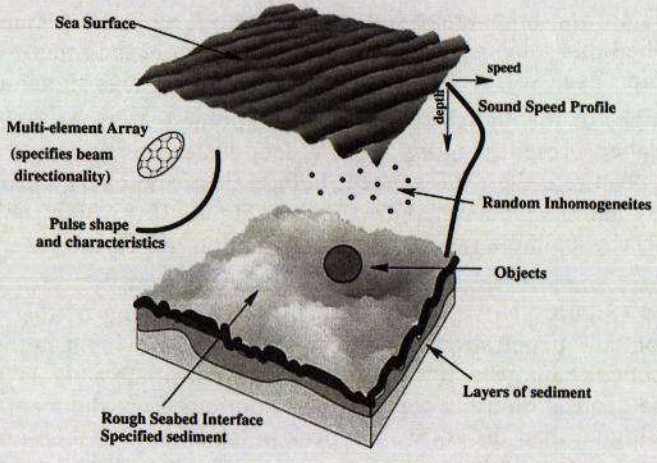

Figure 1. Aspects included in scene description

The generality of the technique provides the basis for a powerful modeling tool as a result of its inherent treatment of all aspects of the propagation of the wave and its interactions with the environment. This tool can then be used to investigate many aspects of ocean acoustics, including the simulation of active sonar systems - the main subject of this paper. To provide flexibility in the system as implemented, the user can fully specify the environment in which the transducers are placed, as illustrated in Figure 1. Setting the appropriate values of the material parameters c, ρ and γ at the relevant positions in the artificial world allows: the water column to have a sound speed profile and random inhomogeneities; the water boundaries to be given particular shapes and roughnesses; and sediment layers and volume inhomogeneities to be included in the seabed. For the transducers, the positions of any number of receivers and transmitters can be defined, and the input pressure signals at each individual transmitter can be specified as arbitrary functions of time, such as a continuous wave (CW) or a pulse.

3. Results

This section will illustrate the scope and generality of the model, and its ability to model many complex aspects of ocean acoustics. Particular emphasis will be placed on the automatic inclusion of multiple reflections and scattering; and on the effects of inhomogeneities in the sediments, which result in volume as well as surface scattering. In each set of experiments the water is defined by $c_w = 1500$ ms^{-1}, $\rho_w = 1000$ ms^{-1} and $\gamma_w = 0$ sm^{-2}, and the environment is restricted to 2D. No source can be defined by a single point because that represents a discrete spatial delta function. This would cause spurious noise after each FFT due to Gibb's phenomenon. The problem is substantially reduced by introducing the source as a weighted combination of a 3x3 region of grid points, with the main element as a point source with identical but half amplitude sources for the four nearest neighbouring points and quarter amplitude sources at the 4 closest diagonal points.

3.1 Channel - Propagation Modelling

There are three aims to this first experiment: first to demonstrate that multiple reflections are an inherent aspect of the PSTD model; second to examine the effect of rough surfaces on these multiple reflections; and third to investigate their effect on sonar signals in shallow water by comparing the signals received from a seabed with and without a sea surface above. This is analogous to shallow and deep-water environments respectively, and in the former case illustrates channel effects.

In order to show the effects of several multiple reflections within the limited area of the simulation (10 m x 5 m), a transmit array is specified to produce a narrow main beam at a depression angle of 59°. This is achieved using 16 elements spaced half a wavelength apart, thus giving a 3 dB beam-width of 6°. Each element transmits a 0.75 ms tapered CW pulse at 13 kHz, giving the pulse a wavelength of 0.115 m. The resulting beam pattern has 7 side lobes to either side of the main lobe and transmits symmetrically to either side of the array, as shown in Figure 2. In the following discussion, the side lobes angled forward of the main lobe are labeled +1 to +7, while those directed more steeply down to the seabed are labeled -1 to -7. A single point receiver is positioned 1 m to the right of the transmit array which places it on the edge of the +6 side lobe, as also shown in Figure 2.

The experiment is run four times to combine two pairs of variations: each environment has a sandy seabed, but the water-air surface is only present in two of them; and each environment contains either completely flat smooth interfaces or rough interfaces. Sand is defined with $c_s = 1767.3$ ms^{-1}, $\rho_s = 1845$ kgm^{-3} and $\gamma_s = 10^{-4}$ sm^{-2} (based on medium sand in [5]), while air has $c_a = 330$ ms^{-1}, $\rho_a = 10$ kgm^{-3} and $\gamma_a = 0$ sm^{-2}. The artificially high density value for air is necessary for the solution to remain stable, but its effect on the reflection coefficient is negligible (<0.4%). The rough surfaces are flat on average (i.e. there are no large scale features) but they do contain small scale roughness. For the seabed this roughness is fractal in nature, while the rough sea surface is characterized by a Pierson-Moskowitz spectrum. Each surface is quantised from a continuous signal and included in Figure 2.

Figure 3 plots the envelopes of the signals received at the point 1 m to the right of the transmit array. With only a smooth horizontal seabed present (Figure 2(a)), a deep-water scenario is simulated. The main beam and side lobes reflect from and penetrate the sand seabed, before all of the energy propagates out of the numerical domain. This is confirmed by the received signal envelope in Figure 3(a) which shows the reflection of side lobe -2 at 3.1 ms; a time confirmed by a simple ray-geometry calculation. No further energy is received, as is expected for a smooth flat seabed.

The fractal rough seabed (Figure 2(b)) gives rise to diffuse scattering of the main beam and side lobes in addition to the reflection from and penetration into the seabed. This is evident in the received signal envelope of Figure 3(b). Detailed ray-geometry analysis of the timings of the multipath arrivals due to the side lobes indicates that the peak in the envelope centred on 3 ms contains contributions from the main lobe and side lobes +1 to -6. This explains why it is 3 dB higher than the equivalent peak in the smooth seabed-only envelope. Side lobes +2 to +5 intersect the seabed at later times, with arrival times centred on 4.0, 4.8, 6.1 and 9.4 ms respectively. Those side lobes whose signals arrive later have more extended footprints on the seabed and this contributes to the continuously received field at later times, in addition to further interactions of forward scattered energy from previous interactions with the seabed.

For the investigation of shallow water channels a smooth horizontal sea surface is introduced over the smooth horizontal seabed (Figure 2(c)), causing the main beam and side lobes to reverberate between the two surfaces. The received signal envelope in Figure 3(c) shows an enhanced peak at 3.1 ms due to the +5 side lobe from the symmetric beam pattern which is emitted from the back of the array and reflects from the sea-air surface. The peak centred at 5.7 ms is due to an off-centre arrival of the -3 side lobe after reflections from the sand and air surfaces. The same side lobe is responsible for the peak at 8.4 ms after another reflection from the seabed. The receiver is now in the centre of the side lobe, and there is a small contribution from the +4 lobe of the reverse-directed beam pattern which arrives off-centre. After a further multiple reflection, the same two side lobes also generate the last peak at 11 ms, with the +4 lobe centred on the receiver and the -3 lobe off-axis.

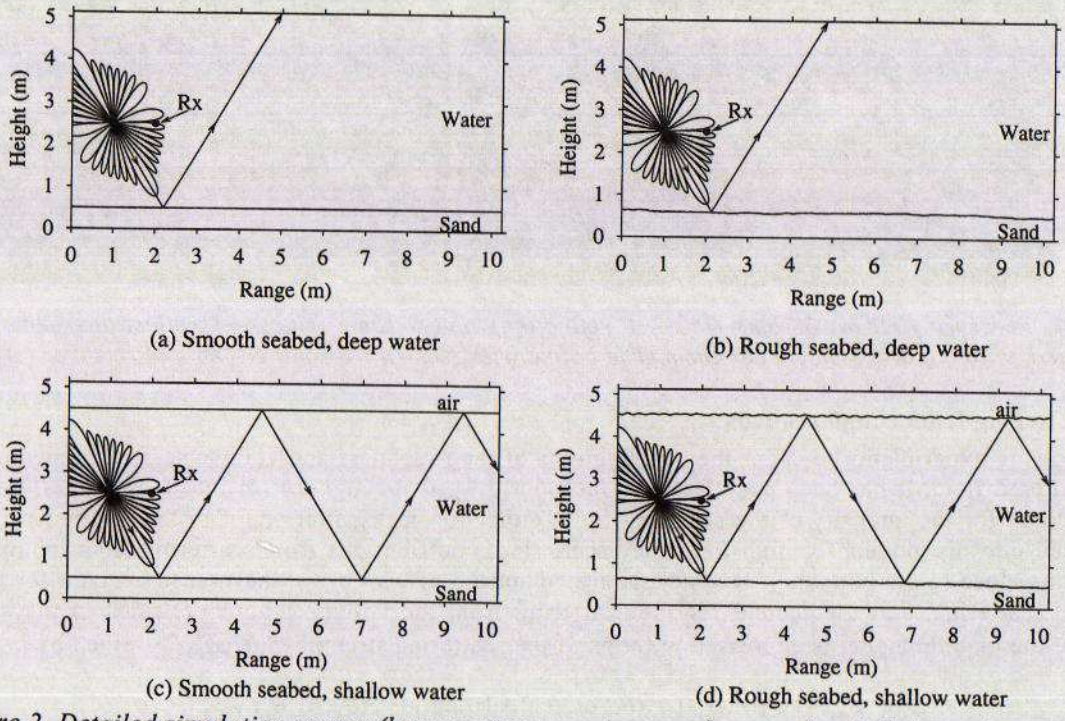

Figure 2. Detailed simulation scenes (beam pattern, receiver, surfaces and main lobe path are marked).

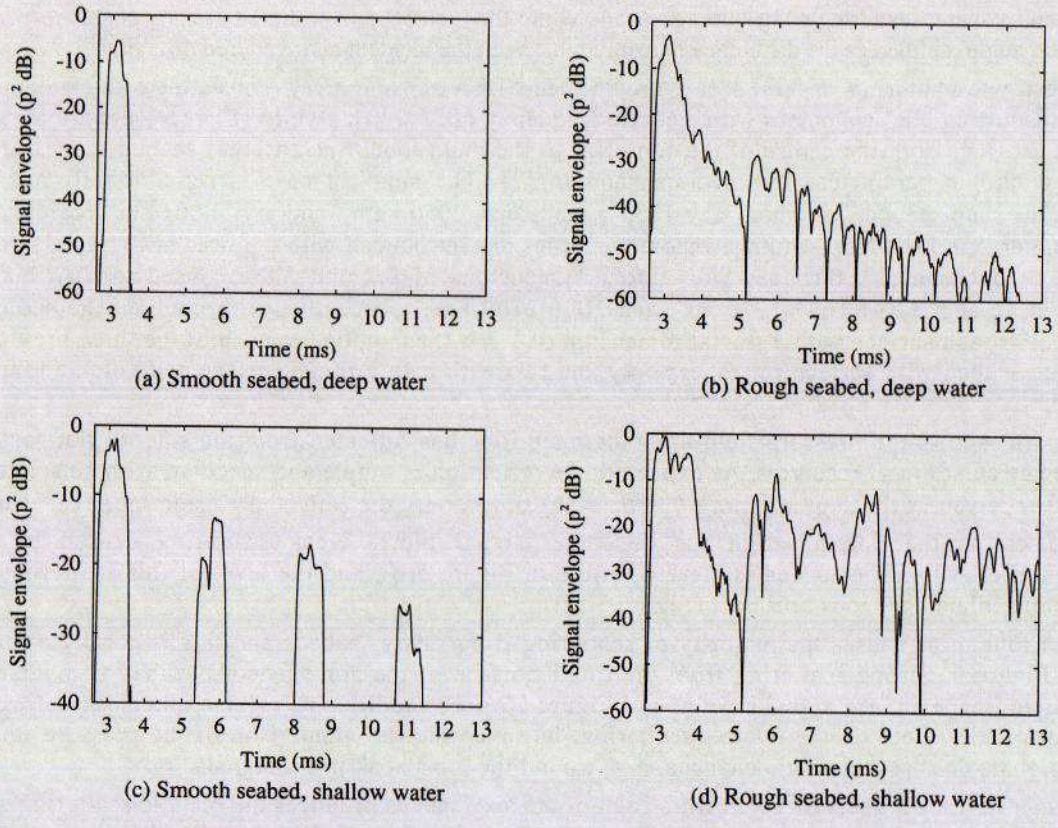

Figure 3. Received signal envelopes (dB re. direct arrival at 1ms which is -30 dB re. main lobe).

In the more realistic shallow water environment where both the seabed and sea surface are rough (see Figures 2(d) and 4), there is increasing complexity of the pressure field with each multiple reflection. The multiple-reflected lobes become gradually more incoherent and lose their sharp structure, and the reverberant field becomes more incoherent and chaotic, although small regions of the field remain coherent. Figure 4 also shows

the penetration of the acoustic field into the sediment. The resulting received signal envelope in Figure 3(d) combines the multiple reflection peaks of Figure 3(c) with the diffuse scattered nature of Figure 3(b).

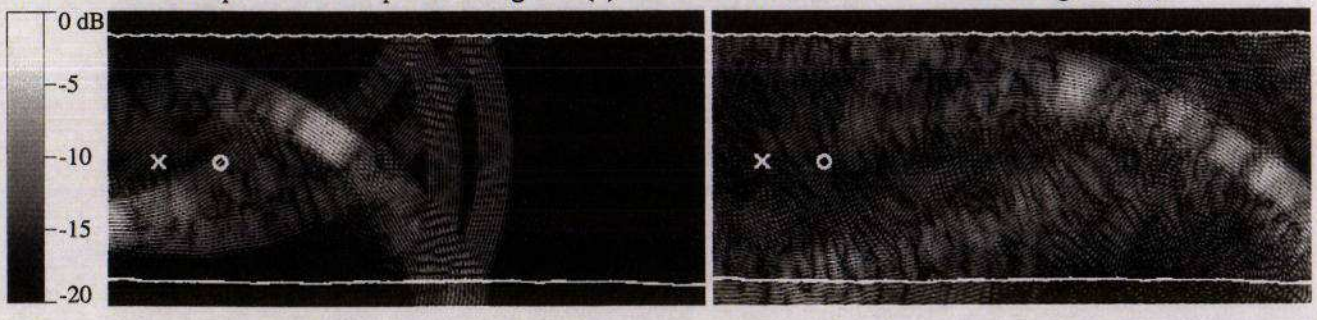

Figure 4. Pressure field at 3.75ms (left - 1 reflection) and 9.75ms (right - 3 reflections). Images are self-normalised, with a 6 dB loss between them. The boundaries (lines), transmitter (X) and receiver (O) are marked.

3.2 Scattering from rough seabeds

The following experiments consider the contributions of the roughness and volume scattering mechanisms on the total scattered field. It has been postulated by Jackson [5,6], that roughness or interface scattering alone cannot fully account for the intensity of the scattered field, either for backscatter or for bistatic scenarios. He therefore introduced into his models for high frequency scattering, contributions from scattering from inhomogeneities in the volume close to the boundary. His models are composed of two terms: the first to account for the roughness interface scattering, and the second for the scattering from the volume inhomogeneities in the sediment. The output of the bistatic model is expressed in terms of the scattering strength $S(\theta_s,\phi_s,\theta_i)$ given by

$$S(\theta_s,\phi_s,\theta_i)=10\log_{10}[\sigma_t(\theta_s,\phi_s,\theta_i)]=10\log_{10}[\sigma_r(\theta_s,\phi_s,\theta_i)+\sigma_v(\theta_s,\phi_s,\theta_i)] \quad (4)$$

where $\sigma_t(\theta_s,\phi_s,\theta_i)$ is the total scattering cross sections per unit area, which is the sum of $\sigma_r(\theta_s,\phi_s,\theta_i)$ and $\sigma_v(\theta_s,\phi_s,\theta_i)$, the roughness and volume scattering contributions; θ_i and θ_s are the incident and scattered grazing angles respectively; and ϕ_s is the bistatic angle, defined as the difference in azimuth between the incident and scattered directions.

To investigate scattering, several scenes are defined with a transmit array (consisting of 8 elements at an angle of 45°) transmitting 0.25 ms pulses with a centre frequency of 26.5 kHz; while 181 receivers are located every 1° around an arc 1 m from the centre of the footprint of the main lobe. Six different seabed scenes are simulated; each based on the parameters for medium sand in [7]. The simplest case is reflection from a smooth flat homogeneous sand seabed, for which c_s = 1732.5 ms^{-1}, ρ_s = 2050 kgm^{-3} and γ_s = 0.001 sm^{-2} (calculated from the loss parameter δ in [5]). Next, volume inhomogeneities are introduced with a power law (fractal) distribution as suggested by Jackson [5]. Surfaces with fractal dimensions of 2.2 and 2.8 are used to distribute correlated variations in c_s and ρ_s (of 1695-1770 ms^{-1} and 2000-2100 kgm^{-3} respectively) throughout the sediment volume (Figure 5). A rough surface with a fractal dimension of 1.3 is then applied to each of the three previous scenes to provide one seabed with surface roughness only and two with both a rough surface and volume inhomogeneities (Figure 6).

Figure 5(a) shows the pressure field after the main lobe has reflected from the smooth flat seabed and as it reaches the circular arc of receivers. As expected, the reflection is simple and specular, with no scattering effects. The signal received at the source point ($\theta_s=\theta_i$=45°) shows only the reflected -2 side lobe (off-centre) and this level is used as the normalisation for the other signal plots. Weak scattering caused by the volume inhomogeneities within the seabed is clearly visible in Figure 5(b), and the level of this scattering is increased with the more inhomogeneous sediment (Figure 5(c)).

Surface roughness causes the majority of scattering from sandy seabeds and this is confirmed by the results shown in Figure 6. Strong scattering from the rough surface of the homogeneous seabed is evident in both the pressure field image and the signal envelope of Figure 6(a). The addition of volume inhomogeneities (Figure 6(b) and (c)) has little effect on the overall scattering, however careful comparison of the pressure images and the received signals does reveal subtle changes, e.g. around the 2 ms peak in the signals.

Analysis of all the signals received from each of the six seabeds produces the bistatic scattering strength plots in Figure 7. Although they are based on a single realisation of each seabed type, and Jackson's bistatic model [5,6] is general and thus represents average behavior, some initial comparisons are useful. Figure 7(a) confirms that higher scattering levels arise from increased volume inhomogeneity, however neither fractal representation is sufficient to account for the volume scattering contribution predicted by Jackson's model. Beyond 65°, the received signals are dominated by the reflected side lobes of the incident beam pattern.

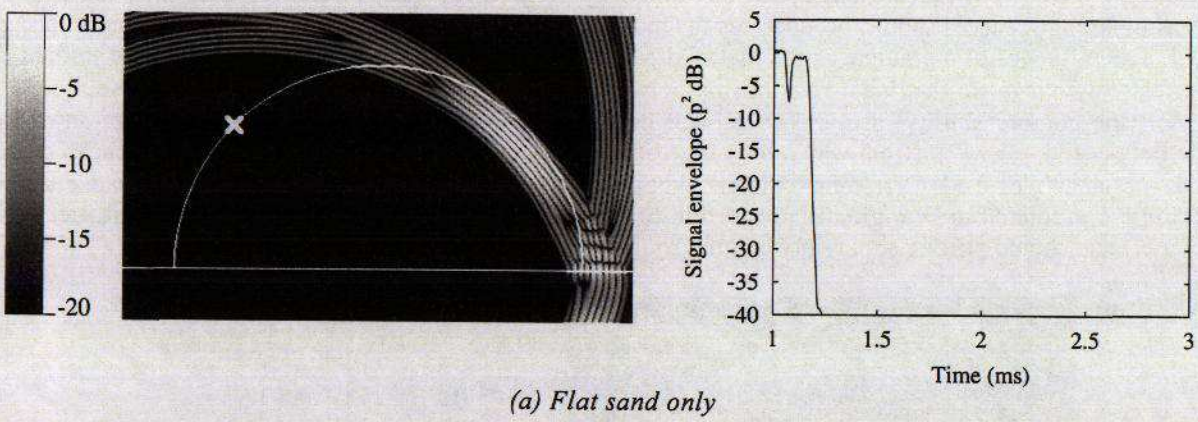

(a) Flat sand only

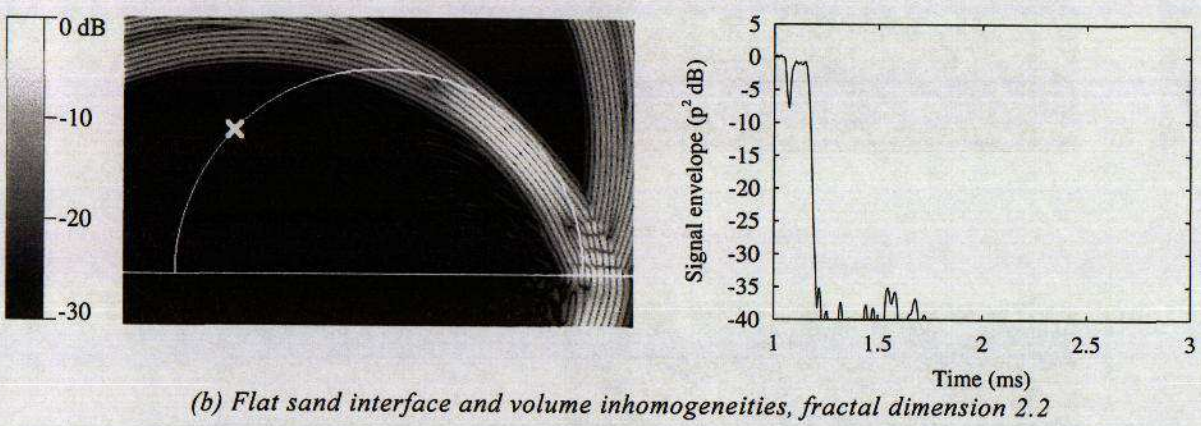

(b) Flat sand interface and volume inhomogeneities, fractal dimension 2.2

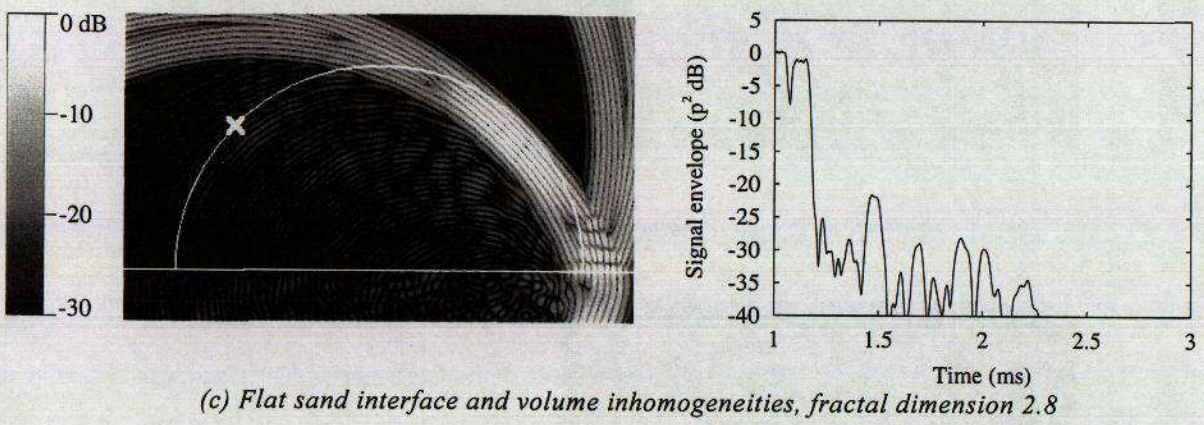

(c) Flat sand interface and volume inhomogeneities, fractal dimension 2.8

Figure 5. (left) Pressure fields at 1.4ms and (right) signals received in the backscatter direction, $\theta_s = 45°$ ($\phi_s = 180°$, $\theta_i = 45°$). The symbol × marks location of transmitter; receivers are located at 1° increments around arc.

The scattering strengths for the rough seabed models are plotted as a single line labeled, "rough," in Figure 7(b) because they are indistinguishable from each other. It broadly follows the predicted trends, except for the large peak in the range 50-75° which is due to strong scattering of the -2 side lobe. The flat homogeneous sand curve has approximately the correct magnitude in the specular direction, but the transmitted beam pattern has obvious influence. Comparing this to the rough sand curve shows that a rough sediment surface scatters energy out of the specular direction, including a strong component in the backscatter direction.

In comparison with Jackson's model, the interface roughness scattering shown in these experiments is too large in the backscatter direction, while the contribution from the volume inhomogeneities is too small. In addition, complex interference effects are apparent at bistatic angles greater than 165°. These are also apparent in the pressure field images of Figures 5 and 6 at these angles on the arc of receivers.

Future investigations will repeat these experiments on medium sand with many different realisations and

distributions for the sediment roughness and inhomogeneity. Averaging related sets of the resulting bistatic scattering-strength curves should produce results more comparable with the predictions of Jackson's more generic model. The influence of a gradient in the material parameters of the upper sediment layers will be studied, as will the effects of changes to the linear relationship between c_s and ρ_s. The assumption made by Jackson [5] is that ρ_s and K_s (the compressibility) are anti-correlated because sound speed is a slowly varying function of density, while Briggs and Tang [7] (from which the range of values in this study have been taken) state a mean correlation between c_s and ρ_s of 0.51. Different sediment types will also be modelled; silt in particular because the volume scattering is predicted to be a greater proportion of the total. This is especially true in the backscatter direction, and its effects should still be apparent when the rough surface is added.

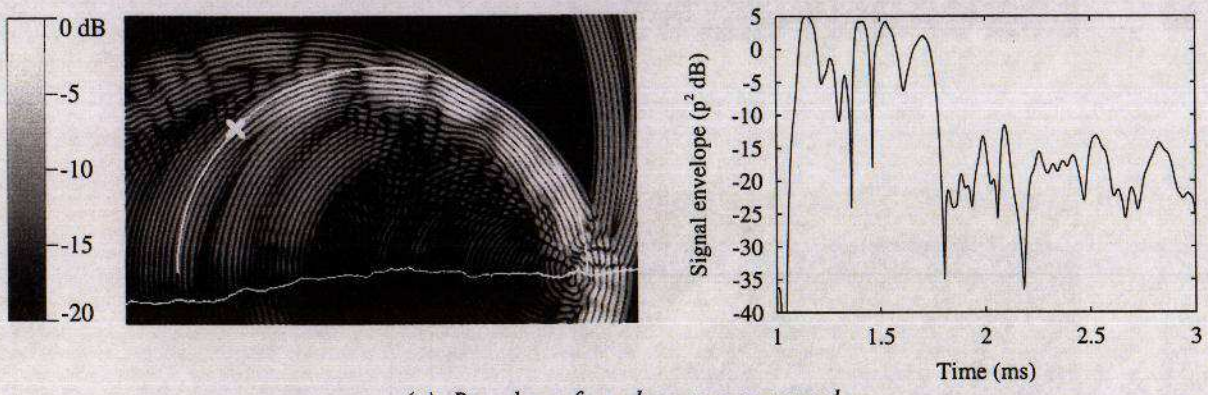

(a) Rough surface, homogenous sand

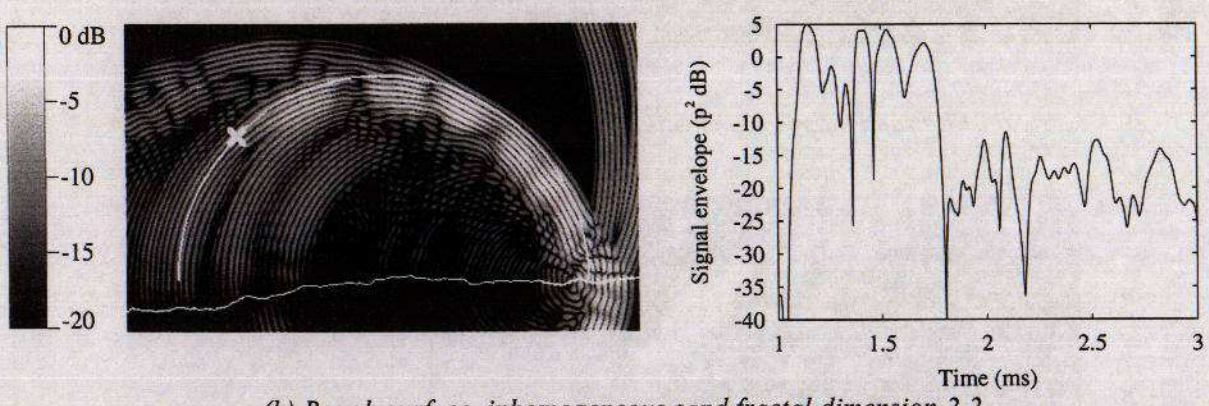

(b) Rough surface, inhomogeneous sand fractal dimension 2.2

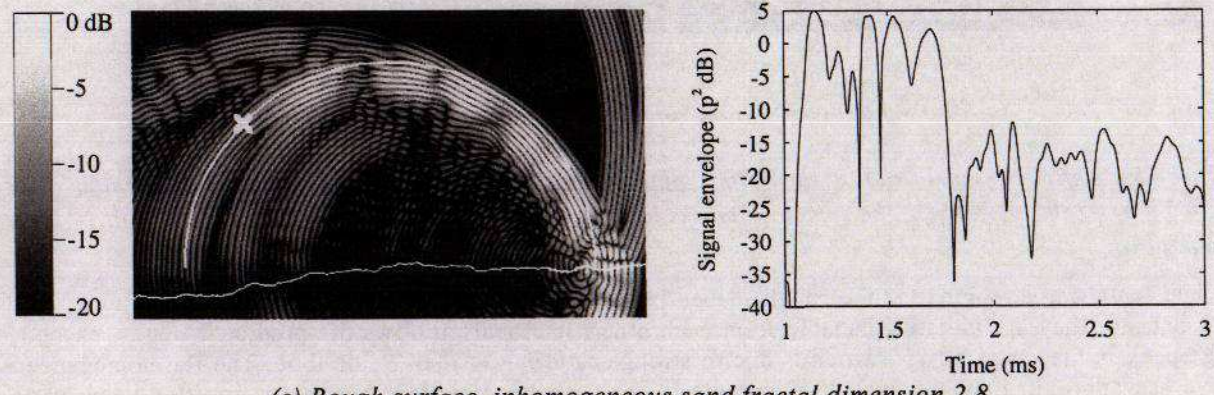

(c) Rough surface, inhomogeneous sand fractal dimension 2.8

Figure 6. (left) Pressure field at 1.4ms and (right) signals received in backscatter direction, θ_s =45 °(ϕ_s =180 °, θ_i =45 °). The symbol × marks location of transmitter; receivers are located at 1 ° increments around arc.

4. Conclusions

This paper has illustrated the use of a PSTD model for ocean acoustics, in particular for simulating active sonar systems. First, the automatic treatment of reflection and transmission at interfaces with different shapes and impedances was shown, including multiple reflections and scattering. The ability of the model to cope with difficult environments was illustrated by the complex reverberant acoustic field displayed in the rough shallow water experiment.

The second set of experiments demonstrated scattering from both the volume inhomogeneities and the rough surface of a sandy sediment, in the latter case with a strength broadly comparable to that predicted by Jackson's well-established generic model. The evidence is not yet conclusive because single seabed realisations have been used, whereas the average behaviour from many statistically similar seabeds is required. Volume scattering is stronger for increased inhomogeneity, although this was only apparent for the smooth flat seabed interface. It is 20-30dB less than expected, probably due to an inadequate sediment representation within the scenes simulated.

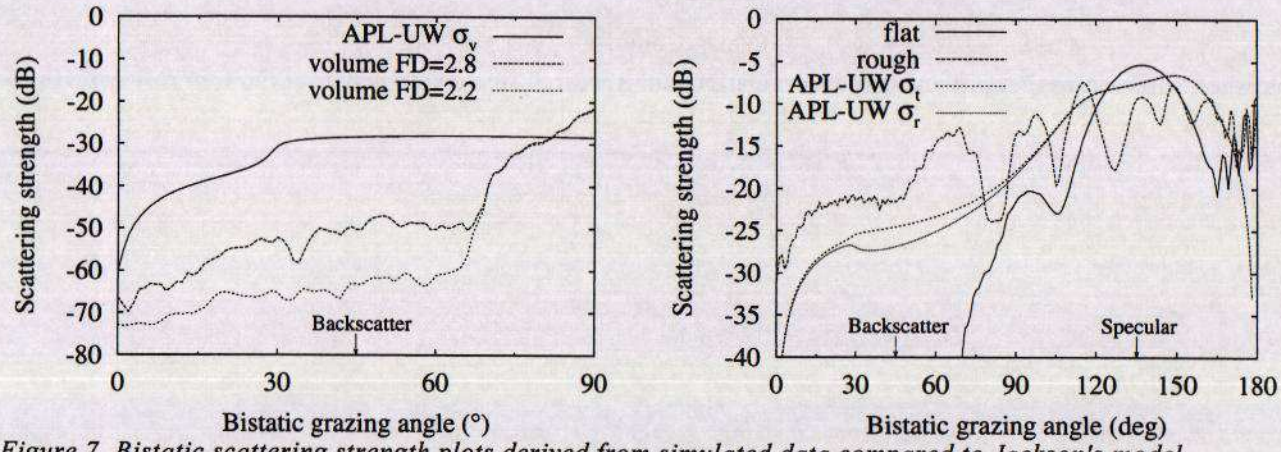

Figure 7. Bistatic scattering strength plots derived from simulated data compared to Jackson's model (a) Volume scattering contribution (b) total (roughness and volume) scattering

All of the results show the flexibility and generality of the PSTD model, and its inherent ability to include coherence, propagation, multiple reflections and scattering. These features, coupled with the unrestricted placement of sources and receivers, make PSTD simulation a powerful tool in sonar and other ocean acoustic modeling. One of the main limitations of the current model is that it neglects shear wave effects, since the discretisation begins with an acoustic wave equation. This limits the model to calculating the scattering only at sedimentary interfaces, rather than solid objects. The importance of shear in the scattering mechanisms will be studied by incorporating elastic properties into the model through use of an elastic form of the wave equation.

Although providing a very flexible and general model, the PSTD model is limited in its range as a result of the computational complexity. This is particularly apparent for high frequency applications since the grid size required to maintain stability is related directly to the wavelength. One solution to this problem is to employ parallel computing techniques which are ideally suited to this type of application. More practical applications suggest the use of hybrid schemes either using a combination of ray tracing and finite difference schemes [8] or using Boundary Integral Methods [9] to translate the solution of the finite difference or pseudospectral model in the detailed region of interest to other parts of the solution.

Acknowledgements

The authors wish to acknowledge the help and support of G. Heald, R. Brothers and S. Page of DERA Bincleaves.

References

[1] Elston GR and Bell JM. Using finite difference methods to model sonar data in complex environments, in *Proceedings of IOA Conference on Sonar Signal Processing* 1998; **20(7)**: 69-76.

[2] Jensen FB, Kuperman WA, Porter MB and Schmidt H. Computational Ocean Acoustics. AIP Press, 1994; pp. 413-429.

[3] Fornberg B. A Practical Guide to Pseudospectal Methods. Cambridge University Press, 1996; pp. 36-47.

[4] Liu QH. The pseudospectral time-domain (PSTD) algorithm for acoustic waves in absorptive media. *IEE Trans. Ultrasonics, Ferroelectrics, Frequency Control* 1998; **45(4)**: 1044-1055.

[5] Jackson DR. Models for Scattering from the Seabed. Proc. Inst Acoust 1994; **16(6)**: 161-172.

[6] Technical Report, Applied Physics Laboratory, University of Washington. APL-UW high frequency ocean environmental acoustic models handbook 1994; APL-UW TR9407: pp. IV-4 - IV-9.

[7] Briggs KB and Tang D. Statistical Variability of Sediment Sound Speed and Density in Fine and Medium Sands, *Proceedings of the 5th European Conference on Underwater Acoustics* 2000; **II**:1265-1270.

[8] Page SJ, Brothers RJ, Murphy KM, Elston GR and Bell JM. A Hybrid Ray-trace/Finite Difference Model for Target Strength Evaluation, *Proceedings 5th European Conference on Underwater Acoustics* 2000; **I**:15-20.

[9] Johnson JM and Rahmat-Samii Y. MR/FDTD: A Multiple-Region Finite Difference Time Domain Method, *Microwave and Optical Technology Letters* 1997; **14(2)**: 101-105.